CrossMark

Anti-corrosion behavior of layer by layer coatings of cross-linked chitosan and poly(vinyl butyral) on carbon steel

Gisha Elizabeth Luckachan · Vikas Mittal

Abstract Anti-corrosion coatings of chitosan were fabricated by layer-by-layer (lbl) addition of chitosan (Ch) and poly vinyl butyral (PVB) on mild carbon steel substrate. Corrosion inhibition of chitosan in lbl coatings was analyzed by electrochemical, spectroscopic and morphological measurements. Sandwiching of chitosan between two hydrophobic PVB layers enhanced its bonding strength and enabled the amine and hydroxyl groups of chitosan to chelate with iron ions that led to the formation of a chitosan stabilized iron oxide passive layer on the metal surface. Effect of chitosan crosslinking on the stabilization process of passive oxide layer as well as the coating stability was studied by incorporating glutaraldehyde in the chitosan layer. The results obtained from electrochemical impedance spectroscopy and Tafel plots clearly showed a superior corrosion protection of lbl coatings generated by 1 % glutaraldehyde incorporation in the middle chitosan layer. SEM and Raman spectra confirmed the formation of passive oxide layer on the metal surface stabilized by chitosan polymer backbone. Improvement in the anti-corrosion properties of PVB_Ch/1 %Glu_PVB coatings were not observed after the incorporation of fillers like graphene and vermiculite in the chitosan layer probably due to the imperfect adhesion of the fillers with the polymeric matrix.

Keywords Chitosan · Poly(vinyl butyral) · Layer-by-layer coating · Passive oxide layer · Glutaraldehyde

Introduction

Corrosion of metals is one of the main destruction processes resulting in huge economic losses, especially in the petroleum, aerospace and automotive industries. Application of organic coatings is most widely used method for the passive corrosion protection of metallic structures (Gonzalez-Garcia et al. 2007; Leidheiser 1982; Walter 1986). Recently, much research effort has been focused on the coatings using renewable resources such as chitin, chitosan, cellulose, polylactide, etc. due to advantages such as cost effectiveness, low toxicity, inherent biodegradability and environment friendliness (Gandini and Belgacem 2002; Derksen et al. 1996). Among these, chitosan (Ch), a linear polyamine consisting primarily of β linked 2-amino-2-deoxy-β-D glucopyranose units, has been widely used for the development of anti-corrosion coatings because of its unique combination of properties such as antimicrobial activity, chemical stability, biocompatibility, and good film forming properties (Carneiro et al. 2012; Pillai et al. 2009). Chitosan can adhere to negatively charged surfaces,

G. E. Luckachan · V. Mittal (✉)
Department of Chemical Engineering, The Petroleum Institute, Abu Dhabi, UAE
e-mail: vmittal@pi.ac.ae

therefore, spontaneously adsorbing on metal or oxide surfaces. It can form complexes with metal ions, and gels with polyanions. The hydroxyl and amine groups on chitosan are reactive and can be used to generate different functional derivatives with desired properties needed for effective corrosion protection (Kumar and Buchheit 2006; Lundvall et al. 2007; Pang and Zhitomirsky 2007; El-Sawy et al. 2001; Sugama and Cook 2000; Ahmed et al. 2012). The controllable release of the active compounds introduced to the chitosan films is also possible, thus, making these films attractive for applications when active corrosion protection is required (Carneiro et al. 2012, 2013; Sugama and Cook 2000; Zheludkevich et al. 2011).

A critical drawback in using chitosan as a corrosion-preventing barrier is its absorption of large amounts of moisture from the atmosphere, thus, forming hydrogels. This transformation not only leads to biodegradation of the film, but also allows moisture to infiltrate easily into the film, causing its failure as a protective coating (Sugama and Cook 2000; Bumgardner et al. 2003). One strategy to overcome this drawback is to associate chitosan with a moisture-resistant polymer. Sugama and Cook (2000) generated water-insoluble chitosan biopolymer coatings on aluminum by grafting synthetic poly(itaconic acid) polymer onto the linear chitosan chains. Dextrin modification of chitosan has also been performed by the same group in an aim to decrease the hydrophilicity and improve the bond strength of chitosan coatings (Sugama and Jimenez 1999). Most of the organic compounds involved in corrosion inhibition contain oxygen, nitrogen and/or sulfur groups, which adsorbed on the metallic surface thereby blocking the active corrosion sites. Since chitosan is naturally rich in such hydroxyl and amino groups, it has a strong potential as corrosion inhibitor, however, a little has been reported about the corrosion inhibition using chitosan. El-Haddad (2014) and Umoren et al. (2013) reported inhibition of copper corrosion and mild steel corrosion respectively in acid medium using chitosan. Aminothiourea modified chitosan was used by Manlin et al. (2014) for the protection of steel in acetic acid. Mohammed and Fekry (2011) reported the protection of steel by chitosan crotonaldehyde Schiff's base in salt solution.

In the current study, stable chitosan coatings on mild carbon steel were generated by layer-by-layer (lbl) addition of chitosan and hydrophobic polymer like poly(vinyl butyral) (PVB) along with analyzing the anti-corrosion performance in 0.3 M salt solution. Glutaraldehyde was used as the cross-linking agent for chitosan in order to reduce the water absorption of chitosan and to enhance coating stability. PVB was selected due its adhesion property along with hydrophobic nature. Lbl coating method was employed to generate a uniform coverage of substrate with chitosan instead of composite film coatings of PVB and chitosan (a method commonly used to improve the performance of hydrophilic polymers). Thus way, PVB over-coating was enabled to prevent chitosan from direct contact with corrosive environment which improved the coating stability and corrosion performance as well. Corrosion inhibition of chitosan in the lbl coatings was analyzed using electrochemical impedance spectroscopy (EIS) and Tafel measurements. Role of small amount of inorganic fillers like graphene and vermiculite in the chitosan layer on the corrosion performance was also studied.

Experimental

Materials

PVB, hydrochloric acid and acetic acid were purchased from Aldrich, Germany and were used as received. PVB (trade name of Butvar B98) had molecular weight of 40,000–70,000 g/mol and specific gravity of 1.1 at 23 °C. Butyral content (expressed as % polyvinyl butyral) was 80 % in the PVB resin used. Chitosan flakes were procured from Bio21, Thailand. Chitosan had a molecular weight of 180,000 g/mol and 90 % degree of deacetylation (DD). Glutaraldehyde was purchased from Fisher Chemicals. Russian vermiculite with a chemical composition of $(Mg,Al,Fe)_3(Al,Si)_4O_{10}(OH)_2Mg_x(H_2O)_n$ was obtained from Thermax, Greinsfurth, Austria. It was received from the supplier as flakes and was subsequently wet ground to the desired particle diameter (partially spherical stacks with average particle size of 5 μm). The grinding operation was performed keeping in mind that the lateral dimensions of the platelets are not milled, however, the thickness of the stacks is reduced so as to generate platelets with high aspect ratio. In the as-supplied form, it contained Mg^{2+} ions on the surface. Single layer graphene platelets were procured from Angstron Materials, USA.

Lbl coatings of chitosan and PVB

0.5 mg chitosan was dissolved in 10 ml of 2 % acetic acid. This mixture was stirred for 24 h to ensure complete dissolution of chitosan in acetic acid. 0.5 mg of PVB was dissolved in 10 ml of methanol. Lbl coating was applied on 5 cm × 3 cm × 2 cm carbon steel coupons by using a dip coater. A layer of PVB was first applied, followed by two layers of chitosan. After drying at 75 °C for 2 h, a final PVB layer was applied. Final coating was cured for 2 h at 90 °C.

PVB_Ch/x %Glu_PVB Coatings

To generate coatings with cross-linked chitosan, 5 ml of x % (where x = 1, 5 and 10 %) glutaraldehyde solution in water were added to 0.5 mg of chitosan dissolved in 10 ml of 2 % acetic acid and stirred for 15 min. Carbon steel coupons coated with PVB as first layer were dip coated two times in the chitosan-glutaraldehyde solution. After drying at 75 °C for 2 h, a final layer of PVB were coated. Final coatings were cured at 90 °C for 2 h. This way, three different coatings were prepared by changing the glutaraldehyde content to 1, 5 and 10 % in PVB_Ch/x %Glu_PVB coating. In order to prepare PVB_Ch/1 %Glu/5 %Gr_PVB composite coating, 0.025 g of graphene was added to 0.475 g of chitosan in 10 ml of 2 % acetic acid solution and sonicated for 24 h. After sonication, 5 ml of 1 % glutaraldehyde solution was added to this mixture and dip coated on the carbon steel coupons using the lbl approach described above. PVB_Ch/1 %Glu/5 %Ver_PVB coating were prepared by following the same procedure using 0.025 g vermiculite instead of graphene.

Immersion test

The edges of the coated coupons were sealed using Nippon epoxy primer. After 24 h drying at RT, samples were immersed in 0.3 M aerated salt solution for standard corrosion analysis.

Electrochemical measurements

EIS measurements and Tafel plots were carried out at RT in a three-electrode corrosion cell consisting of a saturated calomel reference electrode, a platinum counter electrode and lbl coated steel coupons as the working electrode. 0.3 M salt solution was used as electrolyte. All measurements were performed on computerized electrochemical analyzer (supplied by BioLogic, France). 1 cm^2 area of working electrode was exposed to electrolyte and impedance measurements were performed as a function of open circuit potential (E_{OCV}). The selected frequency range was typically from 10^5 to 10^{-2} Hz at AC amplitude of 10 mV. The impedance plots were fitted using an equivalent circuit (given in Fig. 5), where pure capacitances were replaced by constant-phase elements (CPE). The software used for the fitting was EC-Lab V10.39. The capacitance values of the different elements in the equivalent circuit were calculated using the following equation:

$$C = Y_0(\omega_{max})^{n-1}$$

where ω_{max} is the frequency at which the imaginary impedance reaches a maximum for the respective time constant (Zheludkevich et al. 2005; Hsu and Mansfed 2011). Tafel plots were recorded at a scan rate of 0.166 mV/s.

Fourier transformed infrared spectroscopy and Raman spectroscopy

Structural characterization of lbl coatings of chitosan and PVB was carried out using a Bruker VERTEX 70 FTIR spectrometer attached with a DRIFT accessory. IR acquisition was achieved between 4000 and 370 cm^{-1} using OPUS software at 4 cm^{-1} resolution. 128 scans were used for each acquisition. Raman spectra were recorded using LabRAM HR spectrometer (Horiba Jobin–Yvon). Laser light from He/Ne source with wavelength of 633 nm was used for excitation. A long working distance objective with magnification 50× was used to collect the scattered light as well as to focus the laser beam on the sample surface.

Results and discussion

In the current study, coatings of chitosan were generated by layer-by-layer addition of chitosan and PVB on mild carbon steel surface. Final coatings comprised of one layer of PVB followed by two layers of chitosan and final layer of PVB; denoted as

PVB_Ch_PVB. Chitosan layer in the lbl coating were also modified further by crosslinking with glutaraldehyde which is denoted as PVB_Ch/x %Glu_PVB. In addition, the chitosan coatings were also reinforced by addition of 5 wt% of functional fillers like graphene and vermiculite, which are denoted as PVB_Ch/1 %Glu/5 %Gr_PVB and PVB_Ch/1 %Glu/5 %Ver_PVB.

Structure of lbl coatings of chitosan and PVB

Structure of lbl coatings was analyzed using DRIFT spectroscopy. Figure 1 shows the IR spectra of chitosan and PVB, along with PVB_Ch and PVB_Ch/1 %Glu coatings without a PVB top layer. Properties of PVB are characterized by the butyral units as well as hydroxyl and acetal groups (Lian et al. 2014; Tripathy et al. 2003). C–O–C–O-C stretching vibrations of butyral units showed bands at 1167 and 1012 cm^{-1} in the PVB spectra. Less intense peak at

1736 cm^{-1} corresponded to C=O stretching vibration and peaks at 1006 cm^{-1} and 1242 cm^{-1} resulted from C–O–C stretching vibrations of acetate groups. Intense broad band at 3470 cm^{-1} was assigned to –OH stretching vibrations of hydroxyl group, the quantity of which determines the crosslinking capacity of PVB. C-H bending and stretching vibrations of saturated –CH, –CH$_2$ and –CH$_3$ were observed at regions of 2720–2850 cm^{-1} and 1500–1300 cm^{-1} respectively (Lian et al. 2014; Tripathy et al. 2003). Raw chitosan spectrum exhibited an intense broad band at 3477 cm^{-1} corresponding to axial stretching of O–H and N–H bonds. Bands located at 1667 and 1597 cm^{-1} were assigned to the amide 1 and amide 11 vibrations respectively, small hump at 1543 cm^{-1} corresponded to protonated amine, whereas bands at 1425 and 1384 cm^{-1} resulted from the bending vibrations of methyl and methylene groups respectively. The absorption bands in the range of 1000–1200 cm^{-1} corresponded to the polysaccharide

Fig. 1 IR spectra of raw PVB, raw Chitosan, PVB_Ch coating and PVB_Ch/1 %Glu coating
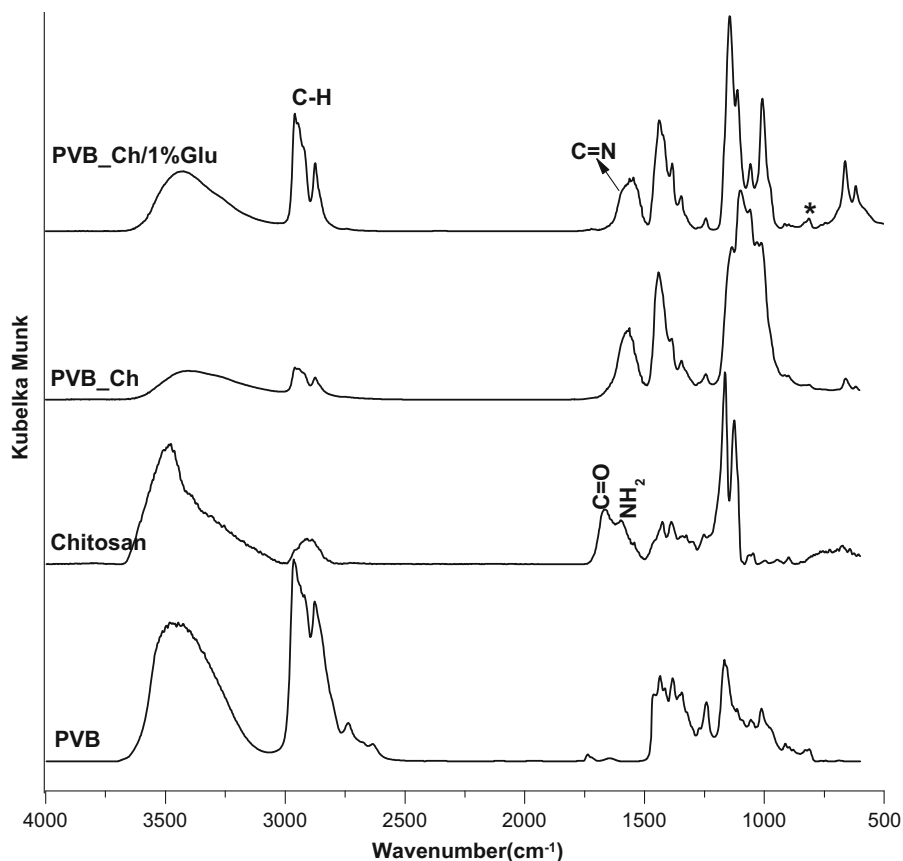
backbone including the glycosidic bonds, C–O and C–O–C stretching vibrations (Carneiro et al. 2013; Li et al. 2013; Sipos et al. 2003; Hernandez et al. 2009).

PVB and chitosan polymers exhibited significant changes in the IR spectra of PVB_Ch coating. Hydroxyl and amine vibrations of PVB and chitosan at around 3470 cm^{-1} became less intense and amide carbonyl vibration of chitosan at 1640 cm^{-1} disappeared almost completely. Taking these changes into account, it can be assumed that PVB hydroxyl and chitosan amide carbonyl groups reacted to result in crosslinking between the two polymers. Not only the shifting of hydroxyl vibrations to 3400 cm^{-1}, but also the broadening of this band indicated further the chances of hydrogen bond interaction between the two polymers. Incorporation of glutaraldehyde in the chitosan layer introduced a new shoulder band at 1600 cm^{-1}, which was attributed to valence vibrations of C=N bond of azomethin group formed by the crosslinking reaction of chitosan with glutaraldehyde (Li et al. 2013; Oyrton et al. 1999). Moreover, the increase in the number of methylene groups in the cross-linked product, attributed to the glutaraldehyde methylene groups, resulted in the increased intensity of C–H vibrations in the region of 3000–2850 cm^{-1}. Hydrogen bonding between chitosan chains became weak by the crosslinking with glutaraldehyde that was observed from the shift of hydroxyl vibrations to a higher wavenumber of 3433 cm^{-1}, evolution of sharp and well resolved peaks attributed to amine and polysaccharide backbone vibrations below 1600 cm^{-1} and the formation of two separate distinguishable bands at 1560 and 1543 cm^{-1} corresponding to –NH-bridging vibrations and protonated amine respectively (Socrates 1994). These spectroscopic results indicated a crosslinking reaction between PVB, chitosan and glutaraldehyde in the lbl coatings. Based on these results, proposed crosslinking mechanism is shown in Fig. 2.

Anti-corrosion performance of chitosan

In order to analyze the protective behavior of pure chitosan, PVB and chitosan coatings of 3 μm thickness were prepared separately, and EIS experiments were conducted on these coatings along with bare steel in 0.3 M salt solution. The Bode and phase plots of all three samples measured after 2 h immersion in 0.3 M salt solution, given in Fig. 3a, showed a single time
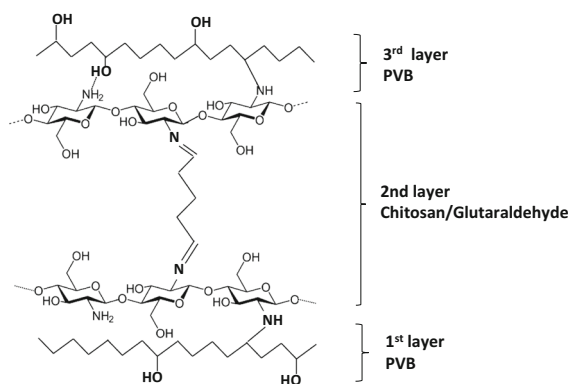

Fig. 2 Schematic representation of crosslinking of chitosan with PVB and glutaraldehyde in the PVB_Ch/x %Glu_PVB coatings

constant at intermediate frequencies (10^0–10^2 Hz). This relaxation process is associated with the double layer capacitance of the electrolyte at the metal surface indicating the corrosion process. However, low frequency Z-modulus, related to the corrosion protection of the coatings, was higher for chitosan coating than PVB coating which showed the anti-corrosion property of chitosan (Qian et al. 2009). It was also observed in the Nyquist plot as increased diameter of the semicircle (Fig. 3b). It has reported that as chitosan is naturally functionalized with amine and hydroxyl groups, these groups can bind or ironically interact with steel via the lone pairs of electrons on the O and N atoms which provide inhibition to steel corrosion (Umoren et al. 2013; Eduok and Khaled 2014). Such an interaction of chitosan functional groups with steel surface has also been observed in the IR spectra of lbl coatings given in Fig. 1. Polysaccharide backbone vibrations of chitosan at 1163 and 1125 cm^{-1} changed to a broad band with multiple peaks at the region of 1200–1000 cm^{-1} in the spectra of PVB_Ch coating which showed the interaction of chitosan hydroxyl groups with steel surface. Free electron doublet on the nitrogen atoms of amine groups are the main sites for the interaction of chitosan with iron ions (Hernandez et al. 2009). But this interaction was not distinguishable because of the overlapping of bands assigned to –NH– bridge vibrations and protonated amine at 1559 cm^{-1}. However, NH deformation band in the chitosan spectra observed at 680 cm^{-1} as a broad hump due to hydrogen bonding formed a well-defined peak at 667 cm^{-1} in the spectra of PVB_Ch coating,
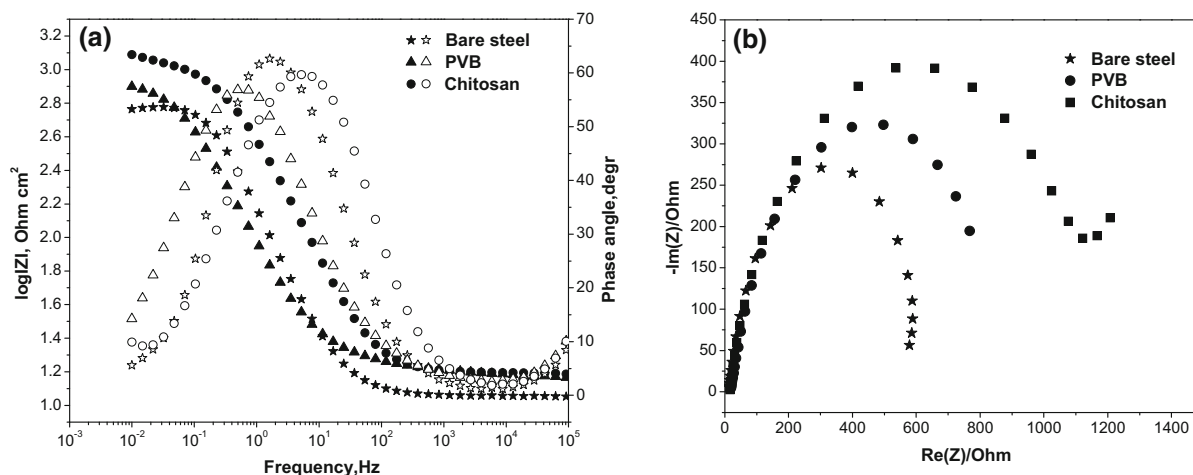
Fig. 3 Bode and Phase plots (**a**) and Nyquist plots (**b**) of bare steel, PVB coating and chitosan coating after 2 h immersion in 0.3 M salt solution

which is attributed to the interaction of chitosan amine groups with metal surface. Chitosan crosslinking with glutaraldehyde reduced intermolecular hydrogen bonding of chitosan chains, and thus released more free hydroxyl and amine groups suitable for chelation with metal ions. It was observed in the IR spectra of PVB_Ch/1 %Glu coating, where NH deformation of chitosan formed a sharp intense band at 663 cm^{-1} and well separated intense hydroxyl bands in 1200–1000 cm^{-1} region. A new band at 812 cm^{-1} attributed to νNH_2 and ρNH_2 also evolved from the interaction of amine group with metal ions (Hernandez et al. 2009). All these changes lead to the probability of chitosan interaction with metal ions through hydroxyl and amine groups which might contribute in the enhanced corrosion protection of underlying metal surface in the lbl coatings. However, corrosion protection of chitosan coatings did not last for long time because of the relatively high affinity of chitosan towards water which opens the pathways for the diffusion of electrolyte ions down to the metal surface.

Corrosion protection properties of lbl coatings of PVB and chitosan

Sandwiching of chitosan in between hydrophobic PVB coatings was achieved to improve the adhesive strength as well as to avoid the direct contact of chitosan with the corrosive medium. The resulting PVB_Ch_PVB coatings were modified further with

the incorporation of different percentages of glutaraldehyde in the chitosan layer and coatings of overall 12 μm thickness were used for anti-corrosion analysis. Corrosion protection of PVB_Ch_PVB coatings in 0.3 M salt solution were monitored by EIS measurements at different times of immersion, and are represented graphically in the Bode and Nyquist plots given in Fig. 4. The impedance at lowest frequency (10^{-2} Hz) in the Bode plot obtained after 2 h immersion was higher by approximately two orders of magnitude than pure chitosan coating. The Bode plot contained two well defined time constants, which are clearly described in the Nyquist plot with two semicircles. Generally, EIS plots of coatings having barrier property show a time constant at high frequency region (Carneiro et al. 2012). Therefore, the time constant at high frequency region (10^5 Hz) in the Bode plot represented the coating response, which might have resulted from the additional barrier provided by the PVB over-coating. The second time constant at low frequency (10^1–10^{-1} Hz) was attributed to the charge/transfer process at the metal electrolyte interface. When the time of immersion increased, low frequency impedance in the Bode plot continued to increase and reached a maximum at 24 h and subsequently started to decrease. Such an electrochemical behavior could be described in terms of an equivalent circuit depicted in Fig. 5. The symbol R$_{sol}$ represents the solution resistance of the bulk electrolyte between the reference and working electrode,
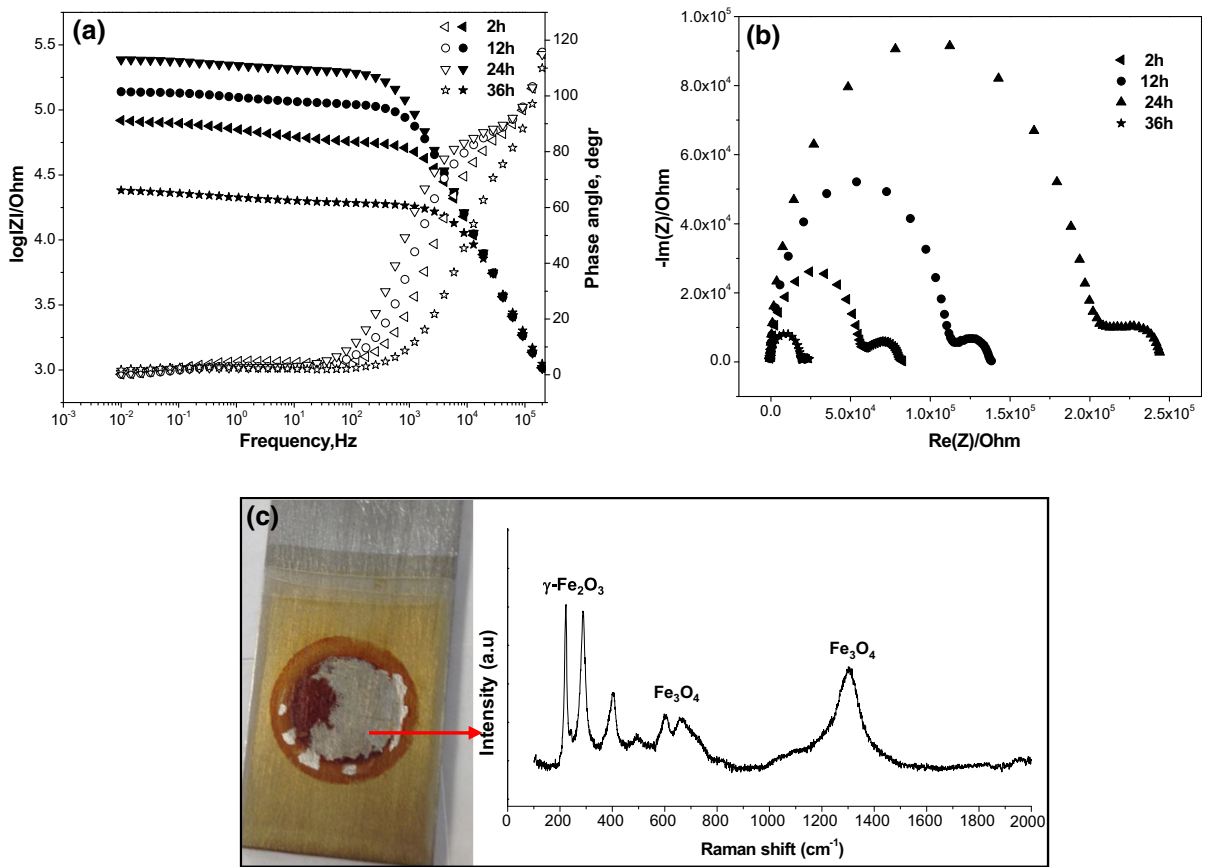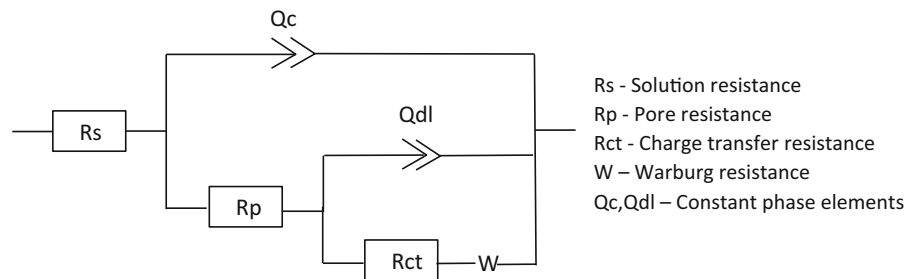
Fig. 4 **a** Bode and phase plots and **b** Nyquist plots of PVB_Ch_PVB coating at different times of immersion in 0.3 M salt solution, **c** Optical photograph and Raman spectra of PVB_Ch_PVB coated steel surface after 24 h EIS and film removal

R_p is the pore resistance of the lbl coating, R_{ct} is the charge transfer resistance, and Q_{dl} and Q_c are the constant phase elements (CPEs). The double layer does not behave as an ideal pure capacitor in the presence of the dispersing effect, so a constant phase element (Q_{dl}) is used as substitute for the capacitor. Dispersing effect of double layer was introduced in the equivalent circuit by the addition of a Warburg element (W). The constant phase element Q_c may be caused by the special property of the lbl coating. There is a chance for interface between the PVB and chitosan layers which contributed to an existence of another interface capacitance-like element reflected by electrical signals. As this interface does not behave as an ideal capacitor, so a constant phase element (Q_c) was used instead. The value of CPE is a function of the

Fig. 5 Equivalent circuit used for EIS modelling

Rs - Solution resistance
Rp - Pore resistance
Rct - Charge transfer resistance
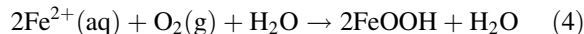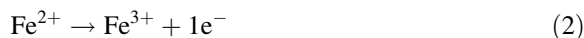W – Warburg resistance
Qc,Qdl – Constant phase elements

angular frequency, ω, and its phase is independent of the frequency. Its admittance and impedance are respectively expressed as

$$Y_{CPE} = Y_0(j\omega)^n$$
$$Z_{CPE} = 1/Y_0(j\omega)^{-n}$$

where Y_0 is the magnitude of the CPE, ω is the angular frequency, and n is the exponential term of the CPE which can vary between 1 for pure capacitance and 0 for a pure resistor (Bao et al. 2011). The electronic parameters obtained from fitting the experimental EIS using the above equivalent circuit are listed in Table 1.

During the immersion in 0.3 M salt solution, pore resistance (R_p) of PVB_Ch_PVB coatings exhibited an increasing trend and after 24 h it reached a value four times higher than the initial value. Since pore resistance is related to the resistance of the electrolyte in pores, cracks, and pits in the coating and reflects barrier property of the coating, it can be suggested that water permeability of PVB_Ch_PVB coatings decreased significantly during the initial exposure time (Latnikova et al. 2012; Rout et al. 2006). At the same time, coating capacitance (C_c) was observed to remain constant over 24 h which indicated that water entered the coating was dispersed throughout the coating instead of localization at the metal/coating interface as free electrolyte (Rout et al. 2006). Further immersion in 0.3 M salt solution increased C_c and decreased R_p values indicating the diffusion of more water/ions into the coating that led to complete degradation of the coating (Rout et al. 2006). The appearance of second loop in the Nyquist plot of PVB_Ch_PVB coatings and the corresponding fitting parameters (R_{ct} and C_{dl}) showed that electrochemical processes started on the metal/solution interface at the early stages of immersion. Corrosion on steel surface involves several oxidation and reduction process given in the equations below (Radhakrishnan et al. 2009):

$$Fe \rightarrow Fe^{2+} + 2e^- \tag{1}$$

$$Fe^{2+} \rightarrow Fe^{3+} + 1e^- \tag{2}$$

$$O_2(g) + 2H_2O + 4e^- \rightarrow 4OH^- \tag{3}$$

$$2Fe^{2+}(aq) + O_2(g) + H_2O \rightarrow 2FeOOH + H_2O \tag{4}$$

As per the equations, a passive oxide layer is formed firstly on steel surface, which is supposed to prevent the underlying metal from further corrosion, similar to other metals like aluminum, copper, etc. (Colreavy and Scantlebury 1995). However, in the case of steel, these oxides are highly porous, which provide a path for the migration of electrolytes down to the metal surface and hence further corrosion occurs below the passive oxide layer. Hence, by stabilizing this oxide layer, it would be possible to slow down the corrosion process on metal surface. Such stabilization of passive oxide layer has been observed in the chitosan coatings. Chitosan is well known for its ability to form stable complexes with transition metal ions. Amino and amide nitrogen, alcoholic and etheric oxygen donor atoms in chitosan can act as a potential binding sites for Fe^{2+} and Fe^{3+} ions (Sipos et al. 2003). It has been reported that iron ion is chelating with 2 mol of amino groups and four moles of oxygen atoms in chitosan, and when pH of the medium changes it oxidizes the iron cations to form chitosan stabilized iron oxides (Hernandez et al. 2009). Therefore, the changes observed in the PVB_Ch_PVB coatings during corrosion analysis indicate that as water/ions reach the metal surface, these facilitate the corrosion process involved in step 1 and 2. The formed Fe^{2+} and Fe^{3+} ions on the metal chelated with chitosan through free amino and hydroxyl groups, which acted as the nucleation sites for the further oxidation. Finally, a passive layer of iron oxide stabilized/covered with chitosan polymer was formed

Table 1 EIS parameters of PVB_Ch_PVB coating at different time of immersion in 0.3 M salt solution

Coating	Exposure time (h)	R_p (Ω cm²)	C_c (F cm²)	Q_c		R_{ct} (Ω cm²)	C_{dl} (F cm²)	Q_{dl}	
				Y_0 (F.s ^.n−1)	n			Y_0 (F.s ^.n−1)	n
PVB_Ch_PVB	2	0.05e6	1.68e−4	2.4e−9	0.92	25930	3.00e−2	11.5e−6	0.57
	12	0.11e6	1.65e−4	2.0e−9	0.93	27240	3.05e−2	12.7e−6	0.60
	24	0.20e6	1.69e−4	1.9e−9	0.94	39637	3.21e−2	7.38e−6	0.62
	36	0.19e5	3.284e−3	4.0e−6	0.88	418	5.85e−2	2.05e−2	0.07

on the metal surface, which protected the metal from further corrosion that contributed to the increased R_{ct} values at 24 h immersion. At the same time, double layer capacitance remained constant indicating the formation of continuous oxide layer on the metal surface. The deposition of iron oxide covered with chitosan backbone effectively blocked the damages on the chitosan coating that might have contributed to an increased R_p values during the initial stages of immersion in salt solution. This passive oxide layer was clearly observed in the optical photograph of PVB_Ch_PVB coating taken after 24 h EIS and film removal (Fig. 4c). Raman spectra of this film showed new bands at 407, 502, 605 and 656 cm^{-1} attributed to Fe_3O_4 oxides and characteristic Raman shifts of γ-Fe_2O_3 at 224, 291 and 1310 cm^{-1} which indicated that the passive layer consisted of Fe_3O_4 and γ-Fe_2O_3 oxides (Wessling 1994; Lu et al. 1995).

Effect of chitosan cross-linking with glutaraldehyde on the protective behavior of lbl coatings

Figure 6a shows EIS spectra acquired after 2 h immersion in 0.3 M salt solution for PVB_Ch_PVB coatings, where chitosan layer was cross-linked by glutaraldehyde incorporation at different percentages. For all the cross-linked coatings, Z-modulus at low frequency was higher than un-crosslinked PVB_Ch_PVB coating. 1 % glutaraldehyde in the chitosan layer increased log Z to 7.6 Ω cm^2, though higher

percentages of glutaraldehyde (10 %) decreased log Z to 5.7 Ω cm^2. However, it was still higher than log Z value of 4.9 Ω cm^2 for un-crosslinked PVB_Ch_PVB coating. The high value of low frequency impedance showed the enhanced corrosion resistance property of PVB_Ch/x %Glu_PVB coatings, which might be due to the formation of cross-linked structure as observed in the IR spectra (Fig. 1) which restricted the penetration of corrosive species to the metal surface by acting as a physical barrier. The barrier response of the coatings was also obvious in the phase plots (in Fig. 6a) with a time constant at high frequency region (10^5 Hz). The identical slope in this frequency region indicated that the three coatings had identical thickness (Maia et al. 2012). The phase angle remained close to 90° for half of the frequency range (10^2–10^5 Hz) covered in the measurement for PVB_Ch/1 %Glu_PVB coating indicating a better barrier property than the PVB_Ch/5 %Glu_PVB and PVB_Ch/10 %Glu_PVB coatings. Second time constant corresponded to corrosion process on metal surface were apparent at 10^0 Hz for 5 % and 10 %Glu modified lbl coatings whereas for 1 %Glu modified coating, it appeared as a small hump at 10^{-1} Hz. Nyquist plots in Fig. 7 also demonstrate these changes in detail.

Nyquist plots of PVB_Ch/x %Glu_PVB coatings were fitted with the electrical circuit presented in Fig. 5 and the fitting results are given in Table 2. Pore resistance (R_p) of the PVB_Ch_PVB coating increased significantly by the addition of 1 % glutaraldehyde in the chitosan layer. Coating capacitance
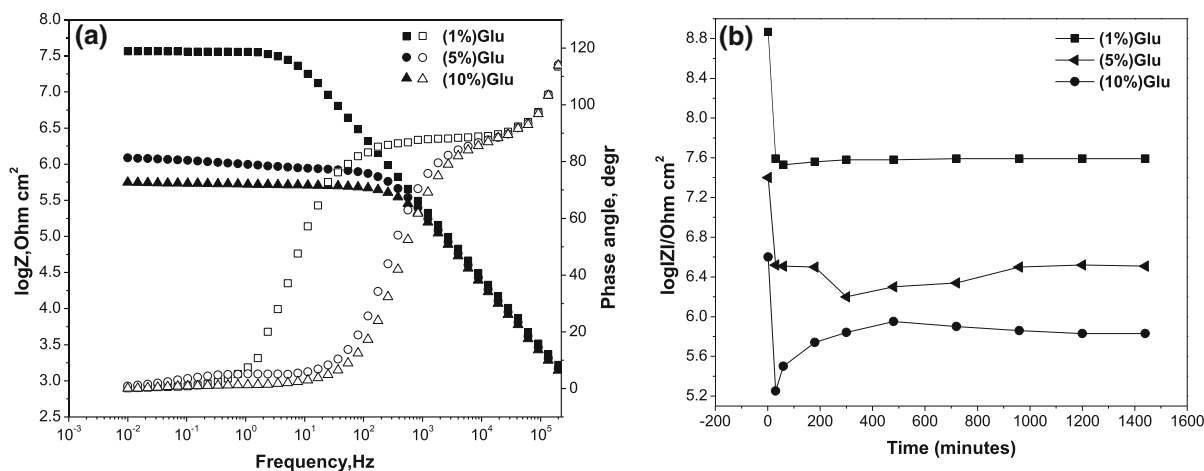

Fig. 6 EIS plots of PVB_Ch/x %Glu_PVB coating having different percentages of glutaraldehyde; **a** Bode and phase plots obtained after 2 h immersion in 0.3 M salt solution and **b** log Z at low frequency from the Bode plot versus time of immersion
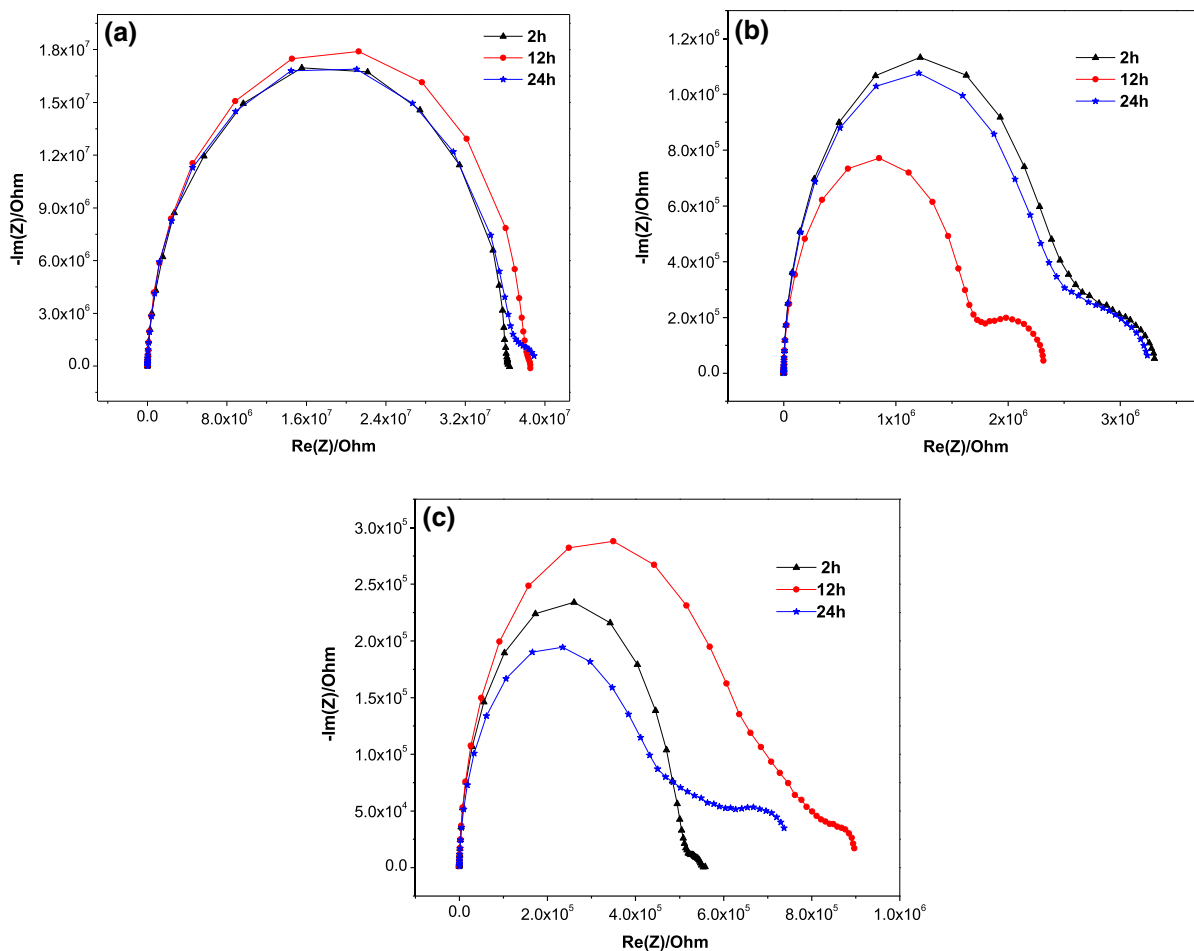
Fig. 7 Nyquist plots of PVB_Ch/1 %Glu_PVB coating (**a**), PVB_Ch/5 %Glu_PVB coating (**b**) and PVB_Ch/10 %Glu_PVB coating (**c**) at different time of immersion in 0.3 M salt solution

was observed to decrease, which indicated that the PVB_Ch/1 %Glu_PVB coating was less permeable to water. However, the capacitance of the coatings increased with increasing glutaraldehyde dosage. These changes can be explained as follows: as the crosslinking agent (glutaraldehyde) content was low, the crosslinking degree was also low, and the molecular chains were in a coiled state which did not form a fixed passage, thus reducing the water absorption. When the glutaraldehyde content in the coating increased, the crosslinking degree of the coating also increased, and the cross-linked networks generated a basic structure which could form a fixed passage for the water molecules (Yu et al. 2011). Water/ion transport through the coatings reduced the pore resistance which was evident from the decreasing R_p

values of PVB_Ch/5 %Glu_PVB and PVB_Ch/10 %Glu_PVB coatings. When the time of immersion was increased, coating capacitance (C_c) and pore resistance (R_p) of PVB_Ch/1 %Glu_PVB coatings increased initially followed by constant C_c for over 24 h whereas R_p decreased slightly. In addition, after an initial decrease, low frequency impedance remained almost constant over the measurement time (Fig. 6b). These results indicated enhanced protective behavior of PVB_Ch/1 %Glu_PVB coating over the neat PVB_Ch_PVB coating. Cross-linking of chitosan with glutaraldehyde reduced the extent of hydrogen bonding between chitosan chains, demonstrated earlier through IR spectra, and released more free hydroxyl and amine groups suitable for the chelation of iron ions that led to the formation of stable passive

Table 2 EIS parameters of PVB_Ch/x %Glu_PVB coatings at different time of immersion in 0.3 M salt solution

Coatings	Exposure time (h)	R_p (Ω cm^2)	C_c (F cm^2)	Q_c		R_{ct} (Ω cm^2)	C_{dl} (F cm^2)	Q_{dl}	
				$Y_{0\ (F.s\ \wedge.n-1)}$	n			$Y_{0\ (F.s\ \wedge.n-1)}$	n
PVB_Ch/ 1 %Glu_PVB	2	36.12e6	8.84e−5	0.75e−9	0.97				
	12	38.81e6	9.57e−5	0.81e−9	0.97	–	–	–	–
	24	37.57e6	9.60e−5	0.82e−9	0.97				
PVB_Ch/ 5 %Glu_PVB	2	0.84e6	0.98e−4	0.97e−9	0.96	0.38e6	4.92e−3	1.25e−6	0.58
	12	2.235e6	1.06e−4	0.99e−9	0.96	1.06e6	2.41e−3	0.41e−6	0.53
	24	2.389e6	1.05e−4	0.99e−9	0.96	0.89e6	3.05e−3	0.49e−6	0.52
PVB_Ch/ 10 %Glu_PVB	2	0.50e6	1.07e−4	1.08e−9	0.96	6.33e4	3.60e−2	9.85e−6	0.43
	12	0.56e6	1.09e−4	1.13e−9	0.96	20.41e4	6.30e−3	1.11e−6	0.44
	24	0.36e6	1.10e−4	1.17e−9	0.95	46.36e4	1.10e−2	1.21e−6	0.30

oxide layer on the metal surface. π electrons in the double bonds of azomethine groups formed by the reaction of chitosan amine with glutaraldehyde carbonyl could also act as an active site of iron oxide stabilization process. Such a corrosion protection was obvious in the digital image of steel surface after removal of PVB_Ch/1 %Glu_PVB coating given in Fig. 8a that showed a uniformly covered grayish layer on the surface. Wessling (1994) and Lu et al. (1995) reported grayish colored layer as resulting from the formation of passive oxide layer on metal surface. SEM images and Raman spectra of these samples were undertaken to analyze the changes on the metal surface. The white lines or scratches observed in the SEM micrograph of bare steel in Fig. 8f, taken before corrosion analysis, were formed by the sand paper polishing process. Raman spectra of this area showed a small hump of iron oxide at 600 cm^{-1} (Fig. 8e), which indicated that acid itching and sand paper polishing removed iron oxide impurities to an extent. Porous corrosion products formed as clusters on the bare steel surface while immersion in salt solution are obvious in Fig. 8g, whereas a less porous uniform film was observed in the SEM image of steel surface after 24 h EIS and removal of PVB_Ch/1 %Glu_PVB coating (Fig. 8d). Raman spectra (Fig. 8e) of this film showed characteristic bands of Fe$_3$O$_4$ oxides at 408, 498, 606 and 659 cm^{-1} and characteristic Raman shifts of γ-Fe$_2$O$_3$ at 225 and 290 cm^{-1} (Wessling 1994; Lu et al. 1995). It can be assumed from these results that infinite array of functional groups on chitosan could act as a chain of nucleation sites from which further growth of iron oxide phase took place. Ultimately, this process resulted in a uniform layer of iron oxide covered with chitosan backbone on the metal surface. In the absence of complexing agent, these iron oxide particles agglomerate and form macroscopic precipitate which was observed on the bare steel surface as clusters of corrosion products. Chitosan steric stabilization prevented agglomeration of iron oxide particles which resulted in a uniformly distributed passive layer on the metal surface beneath the lbl coatings (Qian et al. 2009).

For PVB_Ch/5 %Glu_PVB coating, low frequency impedance (logZ), given in Fig. 6b, initially decreased, followed by an increase and subsequently remaining constant over the measurement time indicating corrosion protection of the coating, though it had a low log Z modulus as compared with PVB_Ch/1 %Glu_PVB coating. It was evident from the C_c and R_p values in Table 2, where the C_c values remained almost constant and R_p increased with immersion time, which indicated that coating prevented the localization of water at the coating/metal interface as free electrolyte. However, high double layer capacitance (C_{dl}) and low charge transfer resistance (R_{ct}) values of PVB_Ch/5 %Glu_PVB coatings after 24 h immersion indicating initiation of active corrosion processes on the metal surface, which are obvious in the optical photographs taken after film removal (Fig. 8b) that showed corrosion products and black coloration. Thick corrosion product was visualized on the metal surface after EIS measurement and removal of PVB_Ch/10 %Glu_PVB coating (Fig. 8c), which
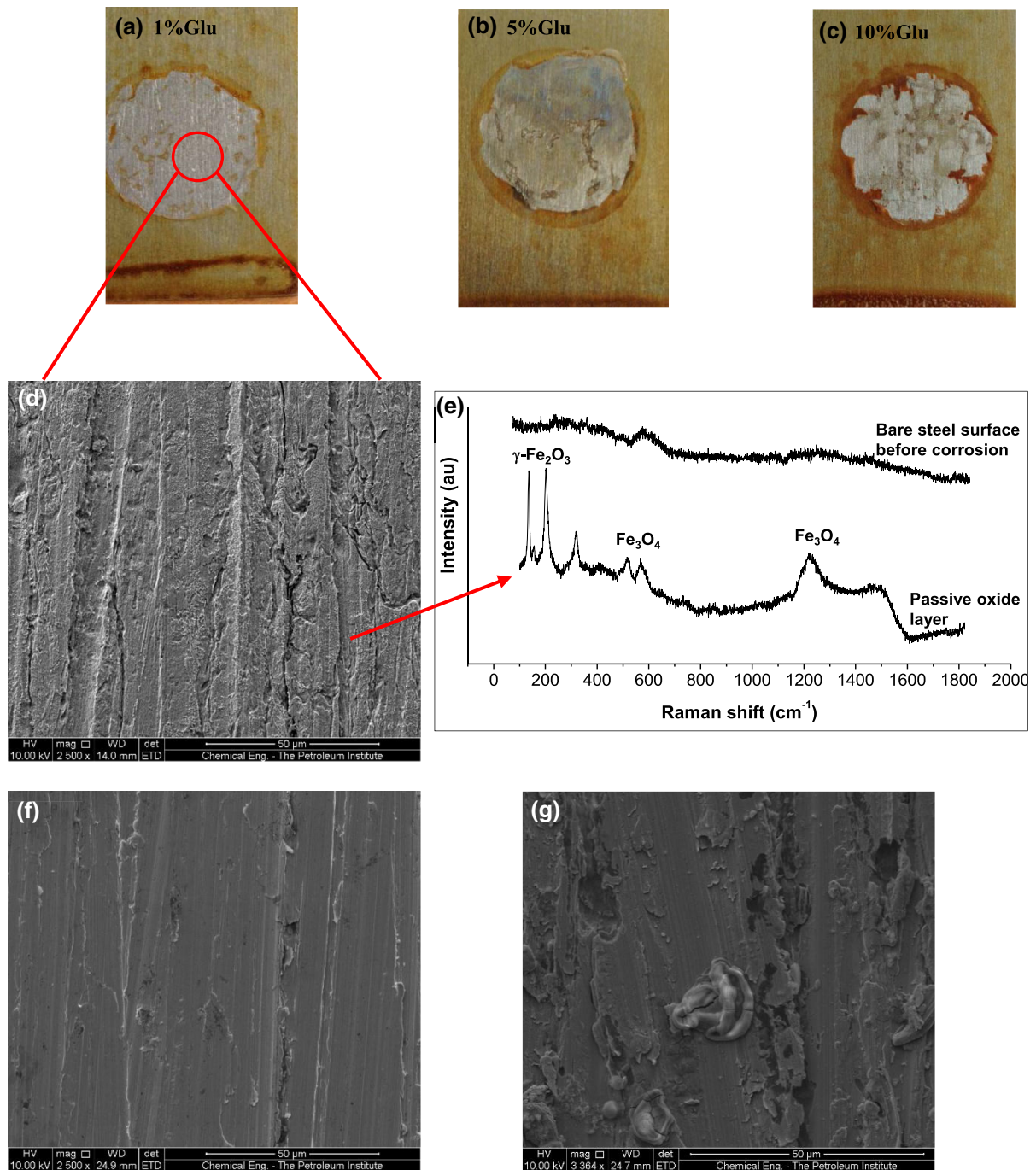
Fig. 8 Optical photographs of **a** PVB_Ch/1 %Glu_PVB, **b** PVB_Ch/5 %Glu_PVB and **c** PVB_Ch/10 %Glu_PVB coated steel surface after 24 h EIS in 0.3 M salt solution and film removal. Diameter of the circle is 1 cm^2. **d** SEM image and **e** Raman spectra of the area marked with red circle on optical photograph of steel surface taken after PVB_Ch/1 %Glu_PVB coating removal. SEM images of bare steel **f** before and **g** after 24 h EIS measurement in 0.3 M salt solution

concluded that the coating did not provide any corrosion protection. It was revealed from the R_p values as well, which decreased with time of immersion. At the same time, C_c showed an increasing trend, as expected. Significantly high R_{ct} values observed at the end of the measurement, obtained by

the protection provided by the thick corrosion products, evidenced the corrosion process on the PVB_Ch/10 %Glu_PVB coated metal surface. The protective behavior of cross-linked chitosan coatings was further evaluated from the Tafel plots displayed in Fig. 9A. For PVB_Ch/1 %Glu_PVB coating, a substantial reduction in both anodic and cathodic current densities was observed. The suppression of the cathodic process was attributed to the barrier property of the coating to the diffusion of water and oxygen. The passive oxide layer stabilized by chitosan polymer backbone suppressed the dissolution of metal from the substrate that resulted in an inhibition of anodic process and a shift of the corrosion potential (E_{corr}) to the positive direction (Radhakrishnan et al. 2009). Further addition of glutaraldehyde shifted E_{corr} to more anodic side supporting the aforementioned EIS data.

Figure 9A also demonstrates Tafel plots of PVB_Ch/1 %Glu_PVB coatings with graphene and vermiculite incorporated in chitosan layer. Bode and phase plots of these coatings taken after 2 h immersion in 0.3 M salt solution are shown in Fig. 9B. Compared with PVB_Ch/1 %Glu_PVB coating, low frequency impedance (log Z) decreased to an order of nearly one and three respectively for PVB_Ch/1 %Glu/5 %Gr_PVB and PVB_Ch/1 %Glu/5 %Ver_PVB coatings which indicated that incorporation of graphene and vermiculite reduced the corrosion resistance of PVB_Ch/1 %Glu_PVB coating. It was earlier reported that well dispersed inorganic particles could increase the length of the diffusion pathways for the gas and vapor molecules in the polymer coatings that could lead to a significant enhancement of corrosion protection of metallic substrates as compared with that of a neat polymer coating (Chang et al. 2012). However, in the present case, the reduced corrosion protection might have resulted from the poor barrier properties due to imperfect adhesion of the fillers to the polymer matrix, which caused the formation of additional diffusion pathways (Latnikova et al. 2012). No interaction between the fillers and the polymer matrix was detected in the IR spectra of these coatings (Fig. 9C) as the characteristic vibrations of PVB_Ch/1 %Glu_PVB coating didn't exhibit any change with the incorporation of graphene and vermiculite in the chitosan layer. The poor barrier properties were evident from the phase angle plot at high frequency region as well. For PVB_Ch/1 %Glu/5 %Gr_PVB coating, the plateau in the high frequency region

reduced slightly to the frequency range of 10^3–10^5 Hz. However, for PVB_Ch/1 %Glu/5 %Ver_PVB coating, the plateau in the high frequency region reduced significantly showing poorer barrier performance due to introduction of new diffusion pathways for the oxygen and water vapor in the polymer coating. Extensive polarity of vermiculite also makes it more susceptible to moisture uptake, thus resulting in deterioration of anti-corrosion performance. The shifting of E_{corr} in the Tafel plots of graphene and vermiculite incorporated coatings to −0.32 and −0.40 V respectively, thus, confirming further the lower extent of corrosion protection of these coatings compared with neat PVB_Ch/1 %Glu_PVB coating (−0.18 V).

Conclusions

Layer by layer addition of chitosan and PVB was employed to generate multi-layer coatings on the carbon steel substrate. Corrosion inhibition of chitosan coatings, brought about by the interaction of metal ions with its functional groups, was confirmed owing to the high Z-modulus at low frequency in the Bode plot. The reduced coating stability of neat chitosan, because of its high affinity towards water, could be successfully controlled by the sandwiching of chitosan layer between two layers of PVB coatings. Incorporation of glutaraldehyde in the chitosan layer in PVB_Ch_PVB coatings introduced a cross-linked structure, resulting in a physical barrier to water and ions reaching the metal substrate. High R_p and low C_c values of PVB_Ch/1 %Glu_PVB coating at the initial time of immersion supported the improved coating behavior. Chitosan backbone was observed to be involved in the stabilization process of passive iron oxide layer on metal surface by iron ion's chelation with free amine and hydroxyl groups of chitosan followed by further oxidation. In other words, an infinite array of donor groups on the chitosan backbone acted as a chain of nucleation sites from which further growth of iron oxide layer took place. Finally, a passive oxide layer sterically stabilized with chitosan backbone was formed that was visually observed as a grayish layer covering the steel surface uniformly. SEM and Raman spectra of the oxide layer confirmed the formation of Fe_3O_4 and γ-Fe_2O_3 oxides on the metal surface. Extent of chitosan crosslinking was the
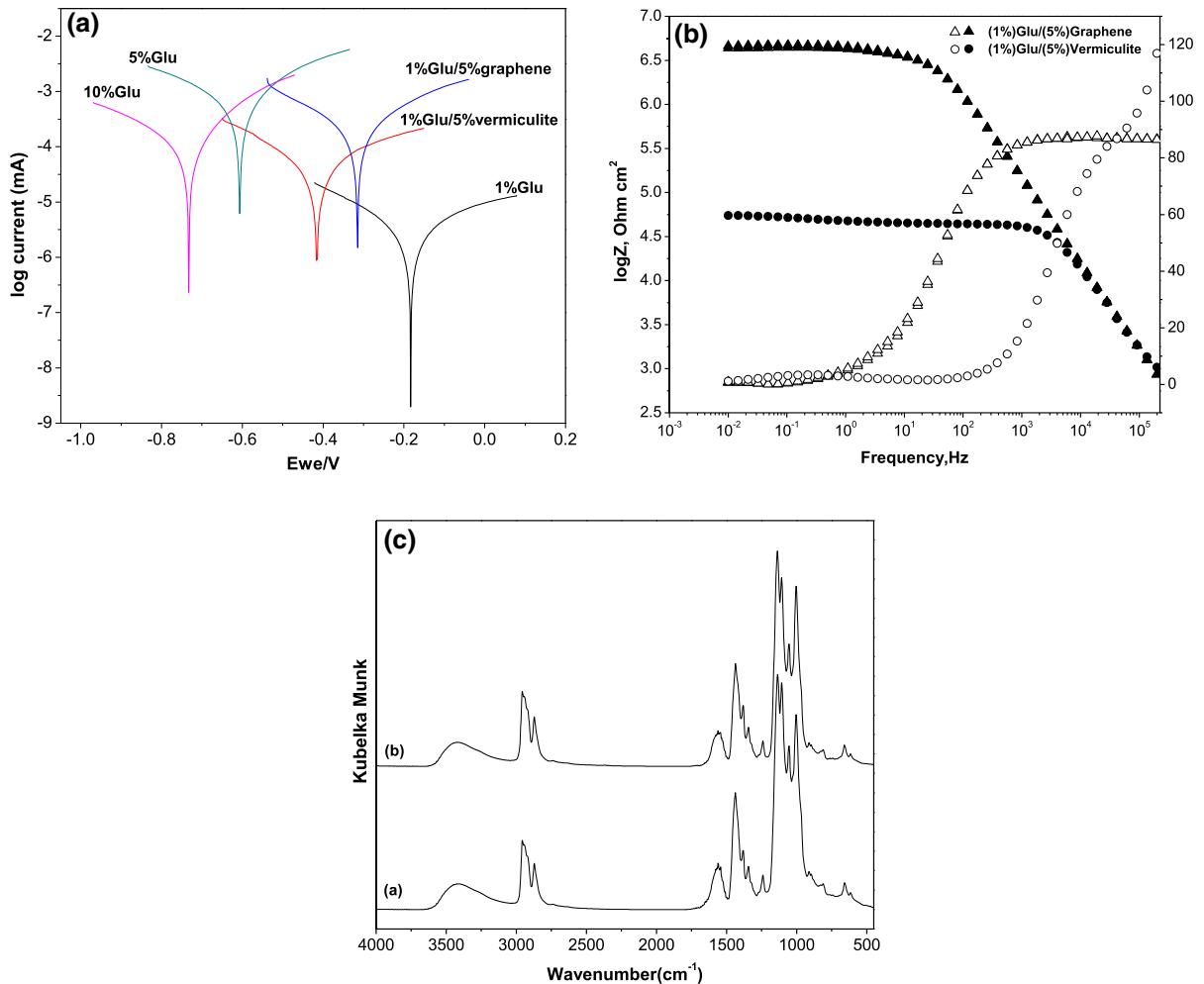
Fig. 9 **A** Tafel plots of PVB_Ch/1 %Glu_PVB, PVB_Ch/5 %Glu_PVB and PVB_Ch/10 %Glu_PVB, PVB_Ch/1 %Glu/5 %Gr_PVB and PVB_Ch/1 %Glu/5 %Ver_PVB coatings recorded after 7 h immersion in 0.3 M salt solution. **B** Bode and phase plots of PVB_Ch/1 %Glu/5 %Gr_PVB and PVB_Ch/1 %Glu/5 %Ver_PVB coatings obtained after 2 h immersion in 0.3 M salt solution. **C** IR spectra of PVB_Ch/1 %Glu/5 %Gr_PVB coating (*a*) and PVB_Ch/1 %Glu/5 %Ver_PVB coating (*b*)

determining factor on the stability and corrosion protection of PVB_Ch/x %Glu_PVB coatings. High glutraldehyde content in the chitosan layer decreased coating performances as the extensive crosslinking provided a fixed path for the penetration of water and ions through the coating. It can be suggested from these results that layer-by-layer addition of chitosan and PVB would be a promising coating method to fabricate stable chitosan coatings. Furthermore, by controlling the extent of crosslinking between the chitosan chains, corrosion inhibition property as well as stability of the coatings can be efficiently improved.

References

Ahmed RA, Farghali RA, Fekry AM (2012) Study for the stability and corrosion inhibition of electrophoretic deposited chitosan on mild steel alloy in acidic medium. Int J Electrochem Sci 7:7270–7282

Bao Q, Zhang D, Wan Y (2011) 2-Mercaptobenzothiazole doped chitosan/11-alkanethiolate acid composite coating:

dual function for copper protection. Appl Surf Sci 257:10529–10534

Bumgardner JD, Wiser R, Gerard PD, Bergin P, Chesnutt B, Marin M, Ramsey V, Elder SH, Gilbert JA (2003) Chitosan: potential use as a bioactive coating for orthopaedic and craniofacial/dental implants. J Biomater Sci Polym Ed 14:423–438

Carneiro J, Tedim J, Fernandes SCM, Freire CSR, Silvestre AJD, Gandini A, Ferreira MGS, Zheludkevich ML (2012) Chitosan-based self-healing protective coatings doped with cerium nitrate for corrosion protection of aluminium alloy 2024. Prog Org Coat 75:8–13

Carneiro J, Tedim J, Fernades SCM, Freire CSR, Gandini A, Ferreira MGS, Zheludkevich ML (2013) Chitosan as a smart coating for controlled release of corrosion inhibitor 2-mercaptobenzothiazole. ECS Electrochem Lett 2:C19–C22

Chang CH, Huang TC, Peng CW, Yeh TC, Lu H, Hung W, Weng CJ, Yang T, Yeh JM (2012) Novel anticorrosion coatings prepared from polyaniline/graphene composites. Carbon 50:5044–5051

Colreavy J, Scantlebury JD (1995) Electrochemical impedance spectroscopy to monitor the influence of surface preparation on the corrosion characteristics of mild steel MAG welds. J Mater Proc Technol 55:206–212

Derksen JTP, Cuperus FP, Kolster P (1996) Renewable resources in coatings technology: a review. Prog Org Coat 27:45–53

Eduok UM, Khaled MM (2014) Corrosion protection of steel sheets by chitosan from shrimp shells at acid pH. Cellulose 21:3139–3143

El-Haddad MN (2014) Hydroxyethylcellulose used as an eco-friendly inhibitor for 1018 c-steel corrosion in 3.5 % NaCl solution. Carbohydr Polym 112:595–602

El-Sawy SM, Abu-Ayana YM, Abdel-Mohdy FA (2001) Some chitin/chitosan derivatives for corrosion protection and waste water treatments. Anti-corrosion Methods Mater 48:227–234

Gandini A, Belgacem MN (2002) Recent contribution to the preparation of polymers derived from renewable resources. J Polym Environ 10:105–114

Gonzalez-Garcia Y, Gonzalez S, Souto RM (2007) Electro-chemical and structural properties of a polyurethane coating on steel substrates for corrosion protection. Corros Sci 49:3514–3526

Hernandez R, Zamora-Mora V, Sibaja-Ballestero M, Vega-Baudrit J, Lopez D, Mijangos C (2009) Influence of iron oxide nanoparticles on the rheological properties of hybrid chitosan ferrogels. J Colloid Interface Sci 339:53–59

Hsu CS, Mansfed F (2011) Concerning the conversion of the constant phase element parameter Yo into a capacitance. Corrosion 57:747–748

Kumar G, Buchheit RG (2006) Development and characterization of corrosion resistant coatings using the natural biopolymer chitosan. ECS Trans 1:101–117

Latnikova A, Grigoriev D, Schenderlein M, Mohwald H, Shchukin D (2012) A New approach towards "active" self-healing coatings: exploitation of microgels. Soft Matter 8:10837–10844

Leidheiser H (1982) Corrosion of painted metals—a review. Corrosion 38:374–383

Li B, Shan CL, Zhou Q, Fang Y, Wang YL, Xu F, Han LR, Ibrahim M, Guo LB, Xie GL, Sun GC (2013) Synthesis, characterization, and antibacterial activity of cross-linked chitosan-glutaraldehyde. Mar Drugs 11:1534–1552

Lian F, Wen Y, Ren Y, Guan HY (2014) A novel PVB based polymer membrane and its application in gel polymer electrolytes for lithium-ion batteries. J Memb Sci 456:42–48

Lu WK, Elsenbaumer RL, Wessling B (1995) Corrosion protection of mild steel by coatings containing polyaniline. Synth Met 71:2163–2166

Lundvall O, Gulppi M, Paez MA, Gonzaleza E, Zagal JH, Pavez J, Thompson GE (2007) Copper modified chitosan for protection of AA-2024. Surf Coat Technol 201:5973–5978

Maia F, Tedim AD, Lisenkov AD, Salak AN, Zheludkevich ML, Ferreira MGS (2012) Silica nanocontainers for active corrosion protection. Nanoscale 4:1287–1298

Manlin L, Juan X, Ronghua L, Dongen W, Tianbao L, Maosen Y, Jinyi W (2014) Simple preparation of aminothiourea-modified chitosan as corrosion inhibitor and heavy metal ion adsorbent. J Colloid Interface Sci 417:131–136

Mohammed RR, Fekry AM (2011) Antimicrobial and anticor-rosive activity of adsorbents based on chitosan Schiff's base. Int J Electrochem Sci 6:2488–2508

Oyrton AC, Monteiro J, Claudio A (1999) Some studies of crosslinking chitosan-glutaraldehyde interaction in a homogeneous system. Int J Biol Macromol 26:119–128

Pang X, Zhitomirsky I (2007) Electrophoretic deposition of composite hydroxyapatite-chitosan coatings. Mater Charact 58:339–348

Pillai CKS, Paul W, Sharma CP (2009) Chitin and chitosan polymers: chemistry, solubility and fiber formation. Prog Polym Sci 34:641–678

Qian M, Soutar AM, Tan XH, Zeng XT, Wijesinghe SL (2009) Two-part epoxy-siloxane hybrid corrosion protection coatings for carbon steel. Thin Solid Films 517:5237–5242

Radhakrishnan S, Siju CR, Mahanta D, Patil S, Madras G (2009) Conducting polyaniline-nano-TiO₂ composites for smart corrosion resistant coatings. Electrochem Acta 54:1249–1254

Rout TK, Bandyopadhyay N, Venugopalan T (2006) Polyphosphate coated steel sheet for superior corrosion resistance. Surf Coat Technol 201:1022–1030

Sipos P, Berkesi O, Tombacz E, St. Pierre TG, Webb J (2003) Formation of spherical iron(III) oxyhydroxide nanoparti-cles sterically stabilized by chitosan in aqueous solutions. J Inorg Biochem 95:55–63

Socrates G (1994) Infrared and Raman characteristics group frequencies, 3rd edn. Wiley, New York

Sugama T, Cook M (2000) Poly(itaconic acid)-modified chitosan coatings for mitigating corrosion of aluminum substrates. Prog Org Coat 38:79–87

Sugama T, Jimenez SM (1999) Dextrine-modified chitosan marine polymer coatings. J Mater Sci 34:2003–2014

Tripathy AR, Chen W, Kukureka SN, MacKnight WJ (2003) Novel poly(butylene terephthalate)/poly(vinyl butyral) blends prepared by in situ polymerizations of cyclic poly(-butylene terephthalate) oligomers. Polymer 44:1835–1842

Umoren SA, Banera MJ, Garcia TA, Gervasi CA, Mirifico MV (2013) Inhibition of mild steel corrosion in HCl solution using chitosan. Cellulose 20:2529–2545

Walter GW (1986) A critical review of the protection of metals by paints. Corros Sci 26:27–38

Wessling B (1994) Passivation of metals by coating with polyaniline: corrosion potential shift and morphological changes. Adv Mater 6:226–228

Yu Q, Song Y, Shi X, Xu C, Bin Y (2011) Preparation and properties of chitosan derivative/poly(vinyl alcohol) blend film crosslinked with glutaraldehyde. Carbohydr Polym 84:465–470

Zheludkevich ML, Serra R, Montemor MF, Yasakau KA, Miranda Salvado IM, Ferreira MGS (2005) Nanostructured sol–gel coatings doped with cerium nitrate as pre-treatments for AA2024-T3: corrosion protection performance. Electrochim Acta 51:208–217

Zheludkevich ML, Tedim J, Freire CSR, Fernades SCM, Kallip S, Lisenkov A, Gandini A, Ferreira MGS (2011) Self-healing protective coatings with "green" chitosan based pre-layer reservoir of corrosion inhibitor. J Mater Chem 21:4805–4812